

# Magnetotransport properties in epitaxial films of metallic delafossite PdCoO<sub>2</sub>: Effects of thickness and width variations in Hall bar devices

Arnaud P. Nono Tchiomo<sup>†,1</sup>, Anand Sharma<sup>†,1</sup>, Sethulakshmi Sajeew,<sup>1</sup> Anna Scheid,<sup>2</sup> Peter A. van Aken,<sup>2</sup> Takayuki Harada,<sup>3</sup> and Prosper Ngabonziza<sup>1,4,\*</sup>

<sup>1</sup>*Department of Physics and Astronomy, Louisiana State University, Baton Rouge, LA 70803, USA*

<sup>2</sup>*Max Planck Institute for Solid State Research, Heisenbergstr. 1, 70569 Stuttgart, Germany*

<sup>3</sup>*Research Center for Materials Nanoarchitectonics (MANA), National Institute for Materials Science, Tsukubashi, Ibaraki 305-0044, Japan*

<sup>4</sup>*Department of Physics, University of Johannesburg, P.O. Box 524 Auckland Park 2006, Johannesburg, South Africa*

(Dated: April 18, 2025)

We report on a combined structural and magnetotransport study of Hall bar devices of various lateral dimensions patterned side-by-side on epitaxial PdCoO<sub>2</sub> thin films. We study the effects of both the thickness of the PdCoO<sub>2</sub> film and the width of the channel on the electronic transport and the magnetoresistance properties of the Hall bar devices. All the films with thicknesses down to 4.88 nm are epitaxially oriented, phase pure, and exhibit a metallic behavior. **At room temperature, resistivity values as low as 6.85 and 8.17  $\mu\Omega\text{cm}$  are achieved in Hall bar devices with channel width  $W = 2.5 \mu\text{m}$  and  $W = 10 \mu\text{m}$ , respectively.** For the 4.88 nm thick sample, we find that while the density of the conduction electrons is comparable in both channels, the electrons move about twice as fast in the narrower channel. At low temperatures, for Hall bar devices of channel width  $2.5 \mu\text{m}$  fabricated on epitaxial films of thicknesses 4.88 and 5.21 nm, the electron mobilities of  $\approx 65$  and  $40 \text{ cm}^2\text{V}^{-1}\text{s}^{-1}$ , respectively, are extracted. For thin-film Hall bar devices of width  $10 \mu\text{m}$  fabricated on the same 4.88 and 5.21 nm thick samples, the mobility values of  $\approx 32$  and  $18 \text{ cm}^2\text{V}^{-1}\text{s}^{-1}$  are obtained. The magnetoresistance characteristics of these PdCoO<sub>2</sub> films are observed to be temperature dependent and exhibit a dependency with the orientation of the applied magnetic field. When the applied field is oriented  $90^\circ$  away from the crystal  $c$ -axis, a persistent negative MR at all temperatures is observed; whereas when the field is parallel to the  $c$ -axis, the negative magnetoresistance is suppressed at temperatures above 150 K.

The delafossite oxides, with general molecular formula of ABO<sub>2</sub> (A=Pd or Pt), have captured significant attention due to their extraordinary electronic and structural properties. The key electronic characteristics include, for example, PtCoO<sub>2</sub> having the highest conductivity per carrier of all known materials and PdCoO<sub>2</sub> exhibiting the longest electron mean free path ( $l_{e(T=4 \text{ K})} = 21.4 \mu\text{m}$ ) for all known oxide materials [1–3]. The huge conductivity results from extremely broad conduction bands based on the  $4d$ - $5s$  electrons of Pd, and the  $5d$ - $6s$  electrons of Pt, whose character is nearly free electron like [3].

We focus on the PdCoO<sub>2</sub> delafossite material. The crystal structure of PdCoO<sub>2</sub> consists of two-dimensional (2D) Pd<sup>+</sup> and [CoO<sub>2</sub>]-layers alternated along the  $c$ -axis as shown in Fig. 1(a). The triangular coordinated Pd site layers are sandwiched between transition metal oxide layers in a stacking sequence [Fig. 1(b) - 1(c)]. The 2D Pd<sup>+</sup> layers are electrically conductive, whereas the [CoO<sub>2</sub>]-layers are electrically insulating. This quasi-2D layered crystal structure results in considerable anisotropy in electrical conduction. In single crystal samples, the room temperature  $ab$ -plane resistivity of  $\rho_{ab} \approx 0.0026 \text{ m}\Omega \text{ cm}$  and  $c$ -axis resistivity of  $\rho_c \approx 1.07 \text{ m}\Omega \text{ cm}$  were reported [3].

For fundamental research perspective, the combination

of above interesting electronic characteristics together with its fascinating structural properties makes PdCoO<sub>2</sub> a promising material candidate for the investigation of fascinating and rich physics of the delafossite materials. **Additionally, PdCoO<sub>2</sub> has a great potential for technological applications. It exhibits exceptional physical properties, such as, a high thermal stability and high optical transparency, which are comparable to those found in transparent conducting oxide compounds employed as electrode material for wide-bandgap semiconductor devices [4, 5].**

Although PdCoO<sub>2</sub> and related metallic delafossites were first synthesized in 1971 [6, 7], PdCoO<sub>2</sub> was largely ignored for decades. It is only in the mid 1990s that Tanaka and co-workers reported the growth of PdCoO<sub>2</sub> and PtCoO<sub>2</sub> crystals [8], as well as the first measurement of the temperature-dependent resistivity of PdCoO<sub>2</sub> [9]. This brought a renewed interest in PdCoO<sub>2</sub> material for studying its basic properties like the thermoelectric power [10–12], electronic structure [13–15] and high anisotropy in structure, conductivity and compression behavior [16–18]. However, the physics of PdCoO<sub>2</sub> has been primarily studied by using single crystal samples. Despite decades of research, these single crystals are still limited in size of  $\approx 3 \text{ mm}$  in diameter [2, 19, 20]. Thus, to allow further studies of its physical properties, particularly as its thickness is decreased down to few unit cells, and the assessment of proof-of-principle spintronic

\* corresponding author: [pngabonziza@lsu.edu](mailto:pngabonziza@lsu.edu)

devices, thin film samples with large area and smooth surfaces are desired.

Recently, the thin films of metallic delafossites with thicknesses down to a few nanometers have been reported by several groups [4, 21–26]. These thin films were grown along the  $c$ -axis direction on substrates with pseudo-triangle lattices, such as  $\text{Al}_2\text{O}_3$  (0001) [27–29] and  $\beta\text{-Ga}_2\text{O}_3$  ( $\bar{2}01$ ) [4, 30, 31]. The  $\text{Al}_2\text{O}_3$  (0001) substrates have been mostly used for the thin-film growth of metallic delafossites [32]. Specifically, epitaxial  $\text{PdCoO}_2$  films have been synthesized using sputtering [33, 34], pulsed-laser deposition (PLD) [22, 24, 35], molecular-beam epitaxy (MBE) [23, 25, 28, 29] and solid-phase reactions of precursors [26].

The magnetoresistance (MR) properties of  $\text{PdCoO}_2$  have been characterized both in bulk single crystals [3] and in epitaxially-grown thin film prepared mostly on sapphire substrates [22–26, 28, 29, 33–35]. The MR data were only reported for a single (one) Hall bar device that was structured by focused ion beam on  $\text{PdCoO}_2$  single crystals [36], and also for a single Hall bar device fabricated on epitaxial  $\text{PdCoO}_2$  films [28, 35, 37]. However, patterning several Hall bar devices of various channel width side-by-side on the same  $\text{PdCoO}_2$  sample offers an advantage over single crystal-based devices as it provides the opportunity to perform comparative study of magnetotransport properties from the same sample, measured in similar conditions [38]. Moreover, this practice is ideal for the exploration of lateral dimensional confinement effects in epitaxial films for tuning their electronic ground states.

In this paper, we report on a combined structural and magnetotransport study of Hall bar devices of various lateral sizes patterned side-by-side on the same  $\text{PdCoO}_2$  thin film. In magnetotransport, we focus on exploring the effects of the film’s thickness ( $t$ ), the variation of the width ( $W$ ) in Hall bar devices as well as the orientation of the magnetic field  $B$  on the MR characteristics. We use pulsed laser deposition (PLD) for the epitaxial growth of these thin films. The growth conditions are optimized to achieve phase-pure metallic delafossite  $\text{PdCoO}_2$  thin films of different  $t$  down to a few nanometers. Subsequent structural analyses using x-ray diffraction (XRD) for unpatterned epitaxial films and high-resolution scanning transmission electron microscopy (STEM) for patterned Hall bar devices, confirm that these films and thin-film devices are epitaxially oriented and phase pure. The temperature dependence of the in-plane resistivity as a function of film thickness show metallic behavior down to  $\sim 4.88$  nm.

For metallic delafossite  $\text{PdCoO}_2$  of various  $t$ , we fabricated side-by-side on the same  $\text{PdCoO}_2$  films several Hall bars of various  $W$ , and then explored their magnetotransport properties. In particular, for two Hall bar devices of channel width  $W = 2.5$  and  $10\ \mu\text{m}$ , we found that the electron mobilities ( $\mu_e$ ), simultaneously extracted from Hall measurements at various temperatures, changed systematically as  $W$  and  $t$  were varied. At 2 K, we extracted

$\mu_e$  values of  $\approx 65$  and  $40\ \text{cm}^2\text{V}^{-1}\text{s}^{-1}$  from the Hall bar devices of  $W = 2.5\ \mu\text{m}$  fabricated on epitaxial films of  $t = 4.88$  and  $5.21$  nm, respectively; whereas the  $\mu_e$  values of  $\approx 32$  and  $18\ \text{cm}^2\text{V}^{-1}\text{s}^{-1}$  were obtained from the devices with channel  $W = 10\ \mu\text{m}$  fabricated on the same respective films. In addition, we find that the magnetotransport is strongly temperature dependent, and present a negative MR that can persist at all temperatures or switch to positive MR at certain temperatures depending on the orientation of the applied magnetic field with respect to the sample  $c$ -axis.

Epitaxial  $\text{PdCoO}_2$  films were deposited on the (0001)-oriented  $\text{Al}_2\text{O}_3$  ( $c\text{-Al}_2\text{O}_3$ ) at a substrate temperature of  $T_{\text{sub}} = 700\ ^\circ\text{C}$  under an oxygen pressure of  $100 - 150$  mTorr in a PLD chamber using the 4<sup>th</sup> harmonic (266 nm) of Nd:YAG laser for ablation.  $\text{PdCoO}_2$  and mixed-phase  $\text{PdO}_x$  targets were alternately ablated to obtain a stoichiometric composition. We prepared films of different thicknesses varying from 4.88 to 11.58 nm. The thickness of the  $\text{PdCoO}_2$  films was determined using the thickness fringes around the  $\text{PdCoO}_2$  (0006) peak in the XRD and the x-ray reflectivity data [21]. The electronic transport properties were measured by using a Quantum Design Physical Property Measurement System (PPMS), where a excitation current of  $I = 1\ \mu\text{A}$  was applied to the Hall bars. The MR properties of the  $\text{PdCoO}_2$  films were studied by changing the orientation of the magnetic field  $B$  such that  $B \parallel c$ , and  $B$  oriented  $45^\circ$  and  $90^\circ$  away from  $c$ . Details on the Hall bar device fabrication are provided in the supplemental material [39].

Figure 1(d) depicts XRD  $2\theta - \omega$  scans of  $\text{PdCoO}_2$  films of different thicknesses. This thickness-dependent analysis exhibits the crystal structure purity of the grown samples. The film reflections form only parallel (000 $l$ ) planes of the bulk crystal structure of  $\text{PdCoO}_2$ , indicating an epitaxial and single phase growth along the  $c$ -axis. Additionally, the clear Laue oscillations observed around the film peaks suggest that the films have smooth surfaces. Note that as the thickness of the films increases (increasing unit cells), the films diffraction peaks become sharper. All these observations are consistent with previous reports on the epitaxial growth of  $\text{PdCoO}_2$  thin films using PLD [22], MBE [23, 25, 28, 29], and sputtering [34].

We studied the structural perfection of the samples by performing symmetric rocking curve  $\omega$  scans for the (0006) film peak as shown in Fig. 1(e). The full width at half maximum (FWHM) values extracted by fitting the rocking curves are plotted in Fig. 1(f). These small FWHM values hint at highly oriented  $\text{PdCoO}_2$  films exhibiting minor out-of-plane misorientation [22, 25, 40]. It is noteworthy that other works on the heteroepitaxial growth of  $\text{PdCoO}_2$  have reported azimuthal mosaicity (in-plane orientation distribution) by recording  $\phi$  scans on asymmetric reflections. It was found that the  $\text{PdCoO}_2$  films exhibit far greater mosaicity in the plane, and grow by forming twin domains which are rotated  $180^\circ$  from one another [see Fig. S1 of the supplemental material] and  $30^\circ$  from the  $\text{Al}_2\text{O}_3$  substrate [22, 23, 25, 34]. Nevertheless,

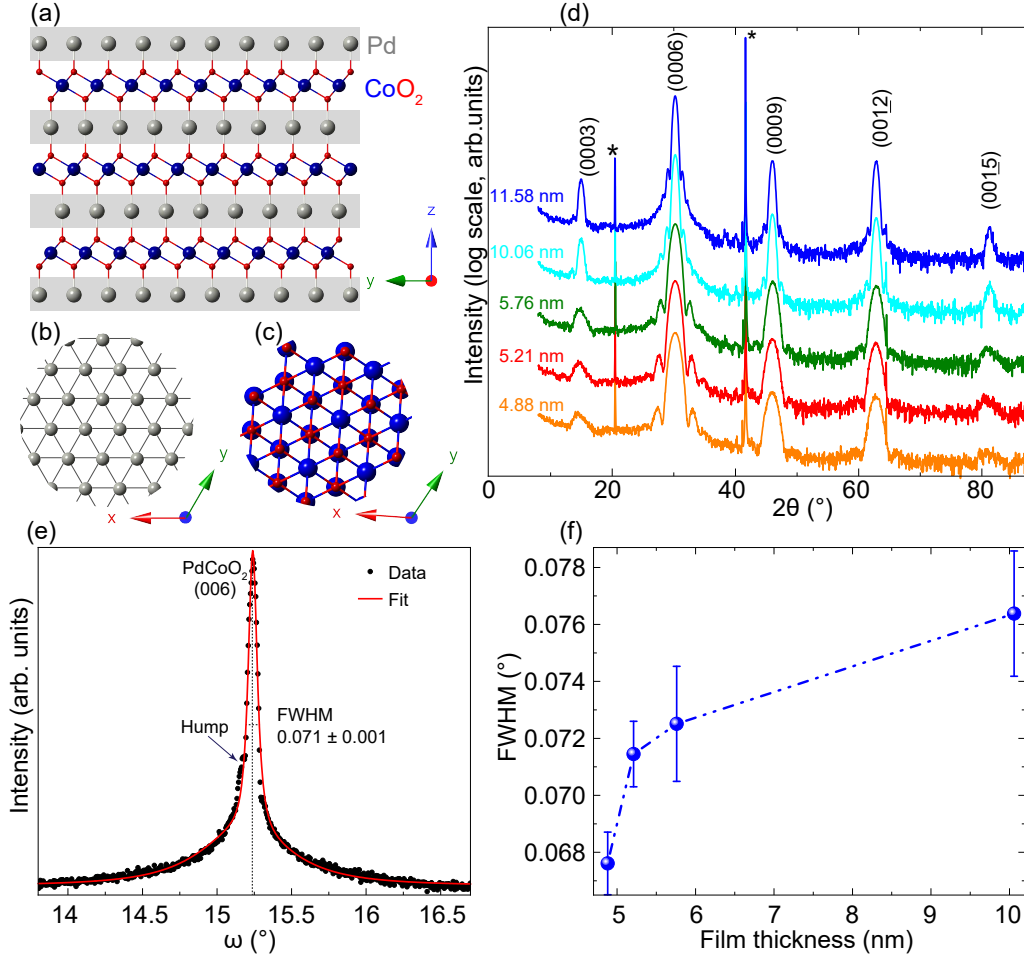


FIG. 1. **Structural characterizations of unpatterned PdCoO<sub>2</sub> films.** (a) A (100) atomic plane view of the crystal structure of delafossite PdCoO<sub>2</sub> presenting alternating stacks of highly conducting Pd and insulating CoO<sub>2</sub> layers. The layers are connected through O–Pd–O dumbbells. Both layers form triangular lattices as shown in the atomic (001) planes in (b) and (c), respectively for Pd and CoO<sub>2</sub>. (d) Thickness-dependent  $2\theta - \omega$  x-ray diffraction patterns of PdCoO<sub>2</sub> epitaxial films grown on (0001)–oriented Al<sub>2</sub>O<sub>3</sub> substrates. The substrate peaks are indicated by asterisks (\*) and the thickness of the films are indicated by the numbers adjacent to each XRD plot. (e) Rocking curve of a representative PdCoO<sub>2</sub> sample acquired around the main (006) film peak, and fitted to extract the full width at half maximum (FWHM). (f) Variation of the FWHM extracted from the (006) peak of the PdCoO<sub>2</sub> films shown in (d). Note the increase of the FWHM with increasing film thickness.

we consistently noted a small hump in the line shape of the main peak in the rocking curves of all the films [see Fig. S2 of the supplemental material]. This could be an indication of an adjacent crystalline domain having a different orientation to the main crystalline block [41]. Our Scanning transmission electron microscopy (STEM) measurements provide evidence of twin boundaries in the PdCoO<sub>2</sub> film as discussed in the following.

Figure 2(c) presents the high-angle annular dark field (HAADF) STEM images of the PdCoO<sub>2</sub> film along the [210] orientation, obtained from a cross-section of a Hall bar device, as illustrated in Fig. 2(b). The magnified HAADF image reveals a sharp and smooth interface between the PdCoO<sub>2</sub> film and the Al<sub>2</sub>O<sub>3</sub> substrate, consistent with the well-defined Laue oscillations observed in the XRD patterns [see, Fig. 1(d)] [25, 42]. Furthermore, the periodic layer stacking of the PdCoO<sub>2</sub> film confirms

the presence of a pure delafossite phase. The crystallographic structures of both the film and substrate can be overlaid on the simultaneously acquired HAADF and annular bright-field (ABF) images, which provide contrast for the lighter elements Al and O.

The STEM images indicate that the epitaxial relationship between the film and substrate is established through the initial [CoO<sub>2</sub>]<sup>−</sup> layer [Fig. 2(c)], which provides the low-energy interface for contact with the substrate, resulting in a stable heterointerface [25, 42, 43]. This is commonly achieved in the growth of delafossite PdCoO<sub>2</sub>, PtCoO<sub>2</sub> and PdCrO<sub>2</sub> materials on the sapphire substrate using both PLD and MBE [22, 25, 28, 29]. Moreover, the HAADF STEM images along the [010] orientation [Fig. 2(d)] reveal domain boundaries, indicating the presence of stacking faults (S) and twin boundaries (T) in the film. The stacking faults correspond to the

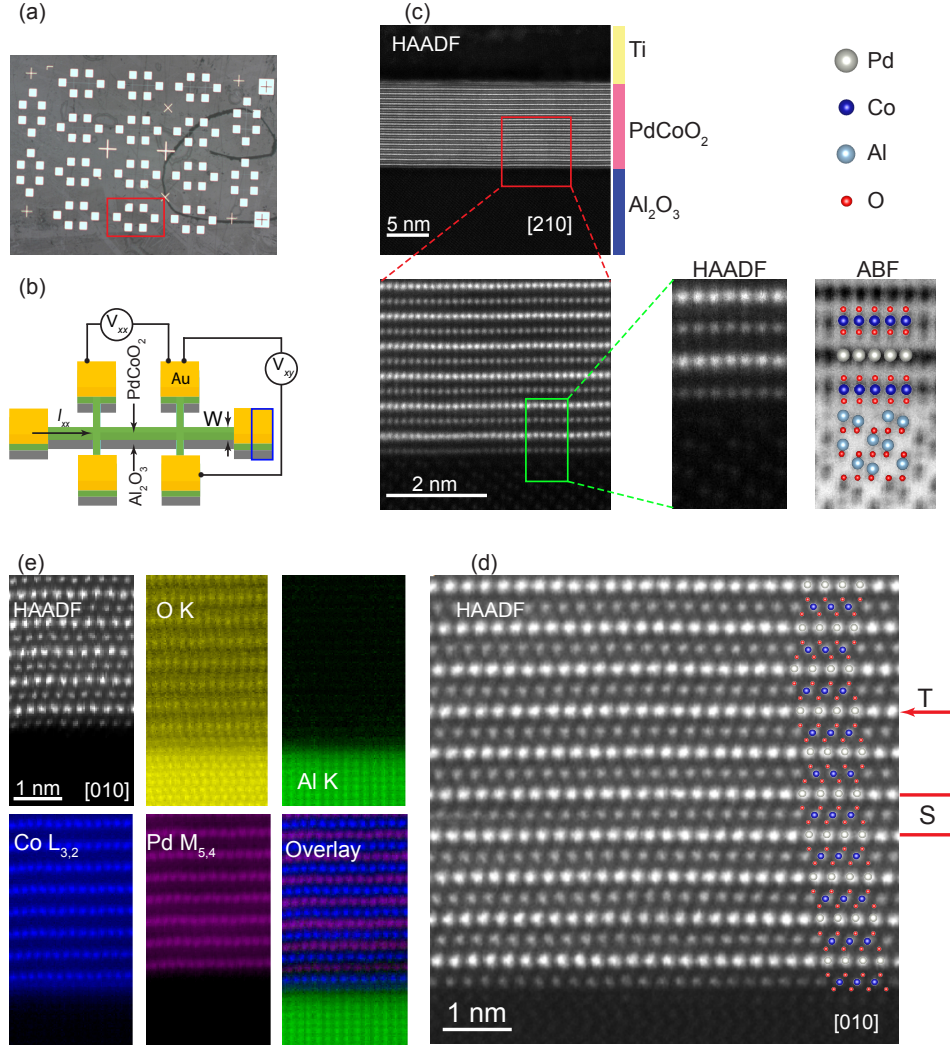


FIG. 2. **Device fabrication and Microstructural characterization of the PdCoO<sub>2</sub> sample grown on (0001)-oriented Al<sub>2</sub>O<sub>3</sub> substrate using PLD.** (a) Optical micrograph image showing a top view of a whole PdCoO<sub>2</sub> sample on which several Hall bar devices of different channel widths (W) were fabricated side-by-side. The channel widths of these devices are  $W = 10\ \mu\text{m}$ ,  $5\ \mu\text{m}$ ,  $2.5\ \mu\text{m}$ ,  $1\ \mu\text{m}$  and  $500\ \text{nm}$ . (b) Schematic illustration of a typical Hall bar device (red rectangle in (a)) indicating the transport measurement configuration. (c) Cross-sectional HAADF-STEM image obtained from a Hall bar device as indicated by the blue rectangle in (b). The enlarged insets show the atomic-scale structure of the delafossite-substrate interface along the [210] orientation of the film with an structural overlay of the atomic models on simultaneously acquired HAADF and ABF images. The HAADF STEM images provide strong contrast for the heavier elements Pd and Co, while the O and Al atomic columns are only visible in the ABF images capturing electrons scattered toward lower angles. (d) HAADF STEM image along the [010] orientation of the film reveals domains with opposing orientations of the CoO<sub>6</sub> octahedra in subsequent [CoO<sub>2</sub>]<sup>-</sup> layers indicating the presence of twins T (red arrow), and stacking faults S. (e) EELS elemental mapping across the PdCoO<sub>2</sub>/Al<sub>2</sub>O<sub>3</sub> interface obtained by extracting the respective edge signals from a 2D spectrum image across the [010] zone axis, indicating a sharp film-substrate interface.

translational displacement of oxygen octahedra in successive delafossite layers; and, the twin boundaries depict the mirrored orientation of the oxygen octahedra in adjacent layers. These features are commonly observed in delafossite thin films grown on *c*-axis-oriented substrates [22, 23, 25, 44].

EELS elemental mapping across the PdCoO<sub>2</sub>/Al<sub>2</sub>O<sub>3</sub> interface, shown in Fig. 2(e), reveals the atomic elemental distribution along the [010] orientation of the film. The

extraction of element-specific energy loss edge signals enables the mapping of the delafossite structure composition. The absence of intermixed layers at the interface suggests that the film exhibits good stoichiometry [45], and confirms its epitaxial growth. The EELS elemental maps further verify that the film nucleates with a [CoO<sub>2</sub>]<sup>-</sup> layer.

The PdCoO<sub>2</sub> samples also exhibit good electrical characteristics over the varying thicknesses as portrayed in



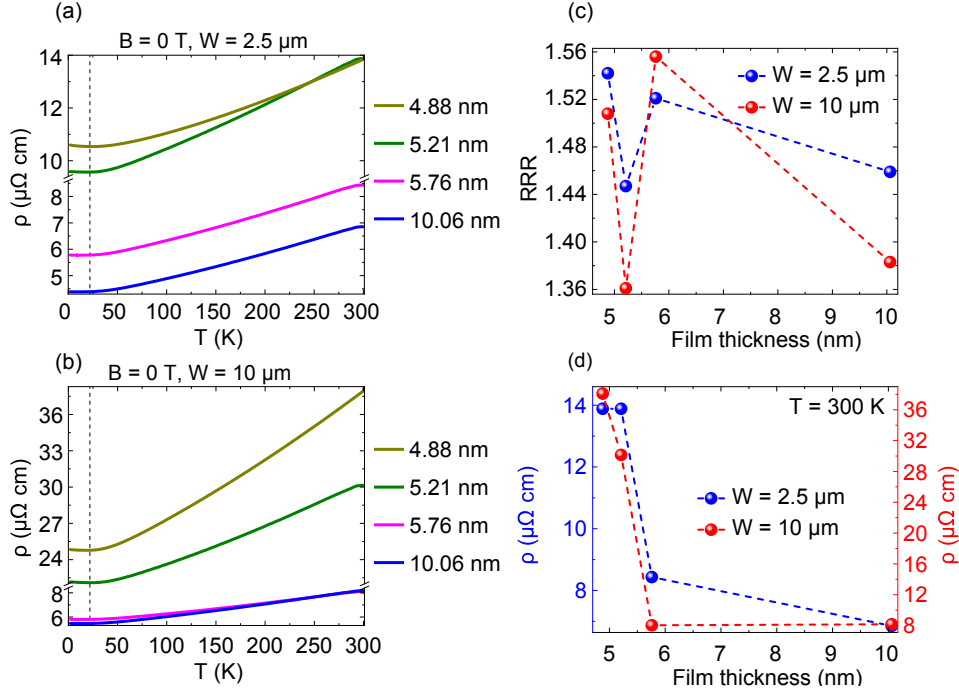


FIG. 3. **Thickness-dependent electronic transport characteristics of PdCoO<sub>2</sub> epitaxial films.** (a) and (b) Temperature dependent resistivity at zero magnetic field for patterned PdCoO<sub>2</sub> Hall bar thin-film devices for a range of thicknesses. The channel widths are (a)  $w = 2.5$   $\mu$ m and (b)  $w = 10$   $\mu$ m. The vertical dashed lines indicate  $T_{\min} = 20$  K. The patterned Hall bar devices in (a) and (b) were fabricated side-by-side on the same PdCoO<sub>2</sub> films in which electronic transport properties were studied. (c) Plot of the variation of the residual resistivity ratio (RRR) as  $\rho_{300\text{ K}}/\rho_{2\text{ K}}$  VS films thickness for both Hall bar widths. (d) Variation of the room temperature (RT) resistivity values as a function of the film's thickness for both Hall bar geometries. The RRR and the RT resistivity values plotted in (c) and (d), respectively, are extracted from (a) and (b). Note that the overall trend with respect to both Hall bar device widths is that the confinement of charge carriers in a narrower channel results in improved electronic properties, as the scattering pathway is reduced.

the temperature dependence of the resistivity at zero magnetic field presented in Fig. 3, for the Hall bar devices with channel widths 2.5 and 10  $\mu$ m. The resistivity is seen to decrease with increasing film's thickness. **We recently demonstrated that a defective interfacial CoO layer forms at the PdCoO<sub>2</sub>/Al<sub>2</sub>O<sub>3</sub> interface [42]. It is likely that this interfacial layer and its associated defects influence the electronic characteristics of thinner films more significantly, explaining the trend observed in the resistivity.** For each sample, the resistivity displays a positive temperature coefficient, consistently for the two Hall bar devices [Fig. 3(a) and 3(b)]. This is indicative of a metallic behavior in all the films over almost the entire temperature range [46, 47]. However, in the low temperature regions,  $T \leq 20$  K, and for all the samples in both device geometries, the residual resistivity is substantially the total resistivity, as the plots are all nearly straight horizontal lines. This saturation is the result of the low temperature effect in nearly pure metallic compounds as outlined by the Matthiessen's rule: To the first approximation, the residual resistivity is governed by scattering of impurities, whose contributions constitute an additive effect to the resistivity and are independent of temperature [48–50]. Nonetheless, deviations from the Matthiessen's rule

are observed at higher temperatures ( $T > 20$  K), as the temperature-dependent component of the resistivity increases in magnitude with decreasing film's thickness [see Fig. S7 of the supplemental material]. Similar thickness-dependent electrical resistivity behavior was reported for MBE grown PdCoO<sub>2</sub> thin films [51]. In addition, the effective mass was found to considerably increase with decreasing film's thickness. It was suggested that, as thinner films exhibit larger surface scattering fraction and higher in-plane defects concentration, disorder-enhanced electron-phonon scattering could be one of the possible mechanisms behind the observed deviations [51]. Note that for bulk pure and nearly pure metals such as Pd, Au, Cu, and Ag, temperature-dependent electrical resistivity analogous to that discussed here has been reported [48].

It is remarkable that the temperature minimum ( $T_{\min} = 20$  K) at which the resistivity starts to plateau (yielding the minimum resistivity) is constant regardless of the thickness of the films and the device width [Fig. 3(a) and 3(b)]. This suggests that the low temperatures transport properties of these films with thicknesses up to about 12 nm are mostly limited by inherent crystallographic defects, which are potentially of equal concentration [48, 49]. In particular, a shallow increase in the resistivity below  $T_{\min}$  associated with disorder-induced

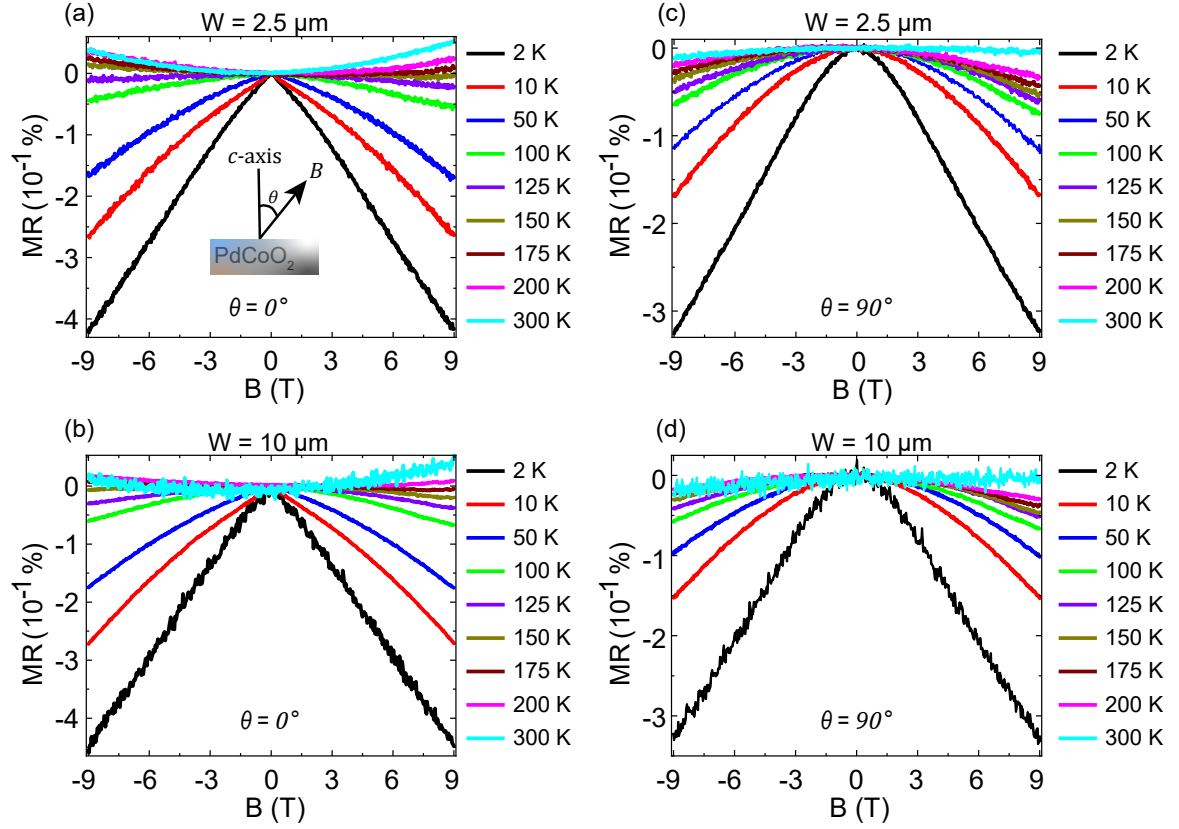


FIG. 4. **Temperature-dependent magnetoresistance (MR) properties of epitaxial PdCoO<sub>2</sub> films measured at different  $B$  orientations.** The data are from two Hall bar devices of channel widths  $W = 2.5 \mu\text{m}$  and  $W = 10 \mu\text{m}$  fabricated on the PdCoO<sub>2</sub> sample with thickness  $t = 4.88 \text{ nm}$ . (a) and (b) MR simultaneously acquired when  $B \parallel c$ , ie,  $\theta = 0^\circ$ . (c) and (d) MR simultaneously acquired when  $B \perp c$ , ie,  $\theta = 90^\circ$ . The insert in (a) shows the orientation of  $B$  with respect to the  $c$ -axis. Note that when  $\theta = 0^\circ$ , the MR present a cross-over from negative to positive at temperatures above 150 K; but when  $\theta = 90^\circ$ , the negative MR persist at all temperatures. Note that through out the magnetotransport measurements,  $B$  is always perpendicular to  $I$ .

localization effects in the PdCoO<sub>2</sub> films was reported in a recent study [23]. It was observed that annealing of the PdCoO<sub>2</sub> films leads to a drop in  $T_{\text{min}}$  and to improved electrical characteristics owing to the reduction of the density of defects in the films [23].

Additionally, since the presence of impurities or defects in metals make these systems more resistive at low temperature [48], the residual resistivity ratio (RRR) for a temperature close to absolute zero ( $\rho_{300 \text{ K}}/\rho_{2 \text{ K}}$ ) represents a very sensitive gauge to structural disorder in the PdCoO<sub>2</sub> films. The maximum RRR of 1.56 for our thickest PdCoO<sub>2</sub> films (11.56 nm) is two orders of magnitude smaller than that of pure bulk single crystals [20], but comparable to those recently reported for PLD and MBE grown PdCoO<sub>2</sub> films at similar thicknesses [22–25] [Fig. 3(c)]. Moreover, the RRR seems to be independent of the thickness of the films. This is contrary to the almost linear trend reported for MBE grown PdCoO<sub>2</sub> films where it was indicated that surface scattering mechanisms including scattering at the twin boundaries and film-substrate interface have a larger contribution to the low temperature electrical resistance [23, 25].

The variation of the room temperature (RT) resistivity values as a function of the film's thickness for both device widths is plotted in Fig. 3(d). **Values as low as 6.85 and 8.17  $\mu\Omega\text{cm}$  are achieved in the narrower and wider devices, respectively. These values are comparable with those reported for the epitaxial growth of PdCoO<sub>2</sub> thin films [22, 23, 25, 51]; and somewhat higher than the RT in-plane value of  $\sim 2.60 \mu\Omega\text{cm}$  obtained in bulk pure single crystals [1, 3, 36].** It is however important to highlight that the comparatively low **in-plane** electrical properties of our PdCoO<sub>2</sub> thin films, especially the low RRR, stem from the presence of additional structural defects in the film such as dislocations, which originate from the large lattice mismatch between the PdCoO<sub>2</sub> film and the Al<sub>2</sub>O<sub>3</sub> substrate [37]. **The  $c$ -axis transport characteristics of the films, which are conceptually challenging to measure would be significantly influenced by these defects, in addition to the insulating state of the CoO<sub>2</sub> layer [15].**

The magnetoresistance (MR) responses of our 4.88 nm thick PdCoO<sub>2</sub> film measured at temperatures ranging

from 2 K to 300 K with the magnetic field  $B \parallel c$  ( $\theta = 0^\circ$ ) and oriented  $90^\circ$  away from  $c$  ( $\theta = 90^\circ$ ) are shown in Fig. 4 for both Hall bar devices. It can be seen that the MR is strongly temperature dependent. When  $\theta = 0^\circ$ , ie, transverse MR [Fig. 4(a) and (b)], the magnetotransport presents two distinct regimes. At temperatures below 150 K, both devices exhibit negative MR which increases with decreasing temperature down to 2 K. This negative MR which is more pronounced at low temperatures ( $\leq 50$  K) could be thought to originate from the weak localization of the electrons in the PdCoO<sub>2</sub> sample. Weak localization is known to be an anomalous quantum phenomenon observed in the transport properties of disordered 2D systems [52]. It has been reported to essentially originates from the quantum interference of the conduction electrons on the defects of the systems [52]. **For our PdCoO<sub>2</sub> samples, which exhibit metallic properties, weak localization is likely a predominant contributor to the observed negative MR. However, at comparable magnetic field strengths, the lineshapes of the negative MR data shown in Fig 4 somewhat differ from those of negative MR data solely attributed to weak localization effects [see Refs. [28, 52]]. This suggest the presence of additional quantum phenomena which, together with weak localization, govern the negative MR observed in our PdCoO<sub>2</sub> films.**

For longitudinal MR measurement ( $B \parallel I$ ) on a ultra-clean PdCoO<sub>2</sub> single crystal sample and for a magnetic field strength up to 9 T, Kikugawa *et al.* [53] observed a negative MR at 1.4 K, similar to the low temperatures MR shown in Fig 4. They argued that this negative MR could not be caused by scattering at magnetic impurities and explained in terms of weak localization effects, given the magnitude of the measured MR, the high purity as well as the non-magnetic property of the sample. This claim was supported by showing that for  $B \perp I$  (transverse MR), large and positive (at all temperatures down to 1.4 K) MR could be achieved. The authors rather attributed the observed negative MR to the emergence of the axial anomaly between the Fermi points of a field induced one dimensional electronic dispersion in PdCoO<sub>2</sub> [53]. **Similarly, our measured PdCoO<sub>2</sub> samples present no evidence of surface magnetism [see Fig. S7 of the supplemental material]. Evidence of surface ferromagnetism was previously reported in an ultrathin (3.8 nm) PdCoO<sub>2</sub> film [37]. The absence of magnetism in our PdCoO<sub>2</sub> samples is possibly due to the mixed termination of the surface, as indicated by the relatively rough surface [see Fig. S1 of the supplemental material]. Nonetheless, given the measurement geometry of the data in Fig. 4 where the current was always perpendicular to the sample  $c$ -axis, we would believe that a different underlying quantum mechanism combined with weak localization could be driving the negative MR in our data.**

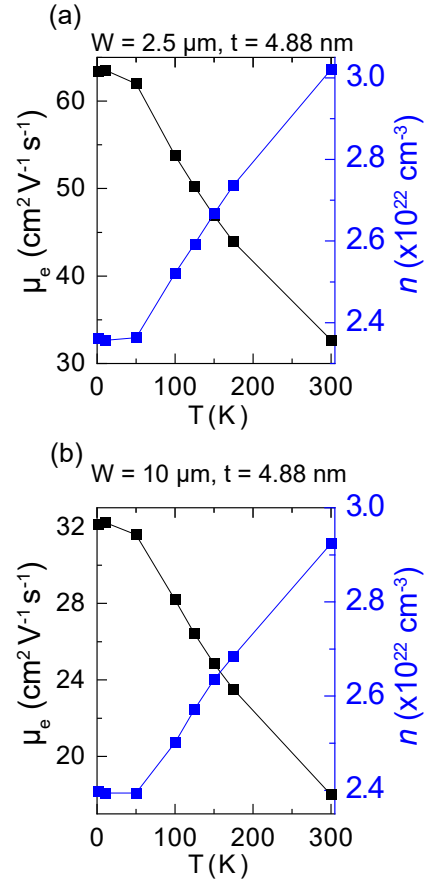


FIG. 5. **Electron mobility ( $\mu_e$ ) and carrier density ( $n$ ) as a function of temperature.** Electronic transport characteristics of the Hall bar devices with channel widths (a)  $W = 2.5 \mu\text{m}$  and (b)  $W = 10 \mu\text{m}$  fabricated on PdCoO<sub>2</sub> epitaxial films of thickness  $t = 4.88 \text{ nm}$ . These data were simultaneously extracted from Hall effect measurements with  $B \perp I$ , i.e.,  $\theta = 0^\circ$ . The narrower channel  $W = 2.5 \mu\text{m}$  yields  $\mu_e$  values that are about twice those of the wider channel  $W = 10 \mu\text{m}$ , while the  $n$  values are comparable.

It is interesting that for the same longitudinal MR measurement by Kikugawa *et al.*, the negative MR is progressively suppressed by increasing the temperature, but does not completely vanishes at the highest temperature of 300 K [53]. This is consistent with the MR response shown in Fig. 4(c) and (d) for MR measurements with  $B \perp c$ , i.e., when  $\theta = 90^\circ$ . These observations suggest that the driving mechanism of the negative MR would not be suppressed when  $B \perp c$ , regardless of the increased thermal energy which triggers resistive mechanisms such as electron-phonon interaction. This is in contrast to the MR response presented in Fig. 4(a) and (b) ( $\theta = 0^\circ$ ,  $B \parallel c$ ). There, as the temperature increases, the lineshape of the MR progresses towards a more quadratic dependence from low temperatures where the MR is negative to temperatures beyond 150 K where the MR becomes positive. Positive MR is believed to be dominated by classical orbital magnetoresistive effects as-

sociated with scattering from impurities and phonons. It is remarkable that these magnetoresistive effects kick in at earlier temperatures in the thickest measured sample,  $t = 11.56$  nm. **This is most probably due to the reduced density of in-plane defects and the small surface scattering fraction of the thicker samples. This provides support for weak localization as the major contributor for the origin of the negative MR.** Positive MR are observed at temperatures  $> 125$  K [see Fig. S3 of the supplemental material]. It is important to highlight that the temperature dependent magnetotransport properties of the 4.88 nm and 5.21 nm samples are comparable, regardless of the orientation of  $B$  [see Fig. 4, and Fig. S4 and S5 of the supplemental material]. Note that a similar temperature-dependent MR crossover was recently reported in a PLD grown PdCoO<sub>2</sub> thin film [37].

Figure 5 depicts the evolution with temperature of the electron mobility,  $\mu_e$ , and the carrier density,  $n$ , of the two Hall bar with indicated channel widths for the same PdCoO<sub>2</sub> sample studied in Fig. 4. Two distinct regimes can be identified for  $n$ : A regime at temperatures between 300 K and 50 K where the carrier densities drop by  $\approx 20\%$  in cooling; and a regime at temperatures below 50 K where the carrier densities are independent of the temperature. These behaviors are consistent with previous reports on the temperature dependence of  $n$  in epitaxial PdCoO<sub>2</sub> films [37, 51, 54]. It is however noteworthy that the strong dependence of  $n$  to high temperatures could be inferred to the level of disorder/defect in the film at high temperatures, which is also associated with sizable changes in the effective mass as discussed above. Hence, it could be that the Hall coefficient at high temperature for this class of material may not reflect the actual carrier density [36, 51].

The extracted  $\mu_e$  range between  $\approx 18$  and  $\approx 65$  cm<sup>2</sup>V<sup>-1</sup>s<sup>-1</sup> in both Hall bar devices from RT to 2 K. This range of electron mobility values is consistent with the small amplitudes of the MR at the field strength of 9 T and for the respective temperatures [37, 55]. In the sample with  $t = 5.21$  nm and for both Hall bar channels [see Fig. S8 of the supplemental material], the carrier densities also drop by  $\approx 20\%$  in a single regime from 300 K to 2 K. The electron mobilities vary from  $\approx 10$  to  $\approx 40$  cm<sup>2</sup>V<sup>-1</sup>s<sup>-1</sup> while cooling from RT down to 2 K, which are consistent with a recent report [37].

In this study, we have reported the structural, mi-

crostructural and magnetotransport properties of Hall bar devices of various widths, fabricated on epitaxial PdCoO<sub>2</sub> films of different thicknesses. We have analyzed two Hall bar geometries of width  $W = 2.5$  and  $10$   $\mu\text{m}$ , all structured into the same delafossite PdCoO<sub>2</sub> thin films of various thicknesses. The PLD prepared PdCoO<sub>2</sub> samples exhibit good structural quality with sharp interfaces that present no signs of atomic interdiffusion. In addition, both Hall bar devices exhibit transport characteristics,  $\rho$ ,  $n$ , and  $\mu_e$ , that are comparable to those reported in the literature. For the device geometries discussed in this work, we found that the narrower Hall bar,  $W = 2.5$   $\mu\text{m}$ , displays slightly better electronic transport performances as compared to the wider  $10$   $\mu\text{m}$  Hall bar. Furthermore, we have demonstrated that the MR properties of the PdCoO<sub>2</sub> samples are strongly temperature dependent, but show no variation with either the thickness of the film or the geometry of the Hall bar device. Moreover, we have noted a persistent negative MR when  $B \perp c$  at all temperatures from 2 to 300 K. For transverse MR,  $B \parallel c$ , the negative MR is suppressed at temperatures above 150 K, and the MR progresses toward a more parabolic dependence, characteristic of classical orbital magnetoresistance. **The lineshapes of our MR data suggest that the origin of the emergence of this negative MR in our PdCoO<sub>2</sub> samples could be attributed to the combining effect of weak localization and some underlying quantum phenomenon.** An attempt to unravel this would be to carry out a systematic study which combines theory and experiment. The results of this study provide additional basis for the understanding of the MR in PdCoO<sub>2</sub> which has proved to be highly dependent on the orientation of the magnetic field, a property that could be relevant to certain applications.

## ACKNOWLEDGMENTS

P. Ngabonziza acknowledges startup funding from the College of Science and the Department of Physics & Astronomy at Louisiana State University; and P. Ngabonziza and A. Sharma acknowledge the invaluable support of Dr. Xiaojian Bai for providing access to his group's PPMS system for electronic transport and magnetoresistance measurements. The authors acknowledge Dr Julia Deuschle for the FIB sample preparation for the STEM investigations.

- 
- [1] C. W. Hicks, A. S. Gibbs, A. P. Mackenzie, H. Takatsu, Y. Maeno, and E. A. Yelland, Quantum Oscillations and High Carrier Mobility in the Delafossite PdCoO<sub>2</sub>, *Phys. Rev. Lett.* **109**, 116401 (2012).
  - [2] P. Kushwaha, V. Sunko, P. J. W. Moll, L. Bawden, J. M. Riley, N. Nandi, H. Rosner, M. P. Schmidt, F. Arnold, E. Hassinger, T. K. Kim, M. Hoesch, A. P. Mackenzie,

- and P. D. C. King, Nearly free electrons in a 5d delafossite oxide metal, *Sci. Adv.* **1**, e1500692 (2015).
- [3] A. P. Mackenzie, The properties of ultrapure delafossite metals, *Rep. Prog. Phys.* **80**, 032501 (2017).
- [4] T. Harada, S. Ito, and A. Tsukazaki, Electric dipole effect in PdCoO<sub>2</sub> &  $\beta$ -Ga<sub>2</sub>O<sub>3</sub> schottky diodes for high-temperature operation, *Sci. Adv.* **5**, eaax5733 (2019).



- [5] P. Ngabonziza and A. P. Nono Tchiomo, Epitaxial films and devices of transparent conducting oxides: La:BaSnO<sub>3</sub>, *APL Mater.* **12**, 120601 (2024).
- [6] R. D. Shannon, D. B. Rogers, and C. T. Prewitt, Chemistry of noble metal oxides. I. Syntheses and properties of ABO<sub>2</sub> delafossite compounds, *Inorg. Chem.* **10**, 713 (1971).
- [7] D. R. C.T. Prewitt, R.D. Shannon, Chemistry of noble metal oxides. II. Crystal structures of PtCoO<sub>2</sub>, PdCoO<sub>2</sub>, CuFeO<sub>2</sub>, and AgFeO<sub>2</sub>, *Inorg. Chem.* **10**, 719 (1971).
- [8] M. Tanaka, M. Hasegawa, and H. Takei, Crystal growth of PdCoO<sub>2</sub>, PtCoO<sub>2</sub> and their solid-solution with delafossite structure, *J. Cryst. Growth* **173**, 440 (1997).
- [9] M. Tanaka, M. Hasegawa, and H. Takei, Growth and Anisotropic Physical Properties of PdCoO<sub>2</sub> Single Crystals, *J. Phys. Soc. Jpn.* **65**, 3973 (1996).
- [10] M. Hasegawa, I. Inagawa, M. Tanaka, I. Shirotni, and H. Takei, Thermoelectric power of delafossite-type metallic oxide PdCoO<sub>2</sub>, *Solid State Commun.* **121**, 203 (2002).
- [11] K. P. Ong, D. J. Singh, and P. Wu, Unusual Transport and Strongly Anisotropic Thermopower in PtCoO<sub>2</sub> and PdCoO<sub>2</sub>, *Phys. Rev. Lett.* **104**, 176601 (2010).
- [12] M. E. Gruner, U. Eckern, and R. Pentcheva, Impact of strain-induced electronic topological transition on the thermoelectric properties of PtCoO<sub>2</sub> and PdCoO<sub>2</sub>, *Phys. Rev. B* **92**, 235140 (2015).
- [13] K. Kim, H. C. Choi, and B. I. Min, Fermi surface and surface electronic structure of delafossite PdCoO<sub>2</sub>, *Phys. Rev. B* **80**, 035116 (2009).
- [14] V. Eyert, R. Frésard, and A. Maignan, On the Metallic Conductivity of the Delafossites PdCoO<sub>2</sub> and PtCoO<sub>2</sub>, *Chem. Mater.* **20**, 2370 (2008).
- [15] K. P. Ong, J. Zhang, J. S. Tse, and P. Wu, Origin of anisotropy and metallic behavior in delafossite PdCoO<sub>2</sub>, *Phys. Rev. B* **81**, 115120 (2010).
- [16] R. Daou, R. Frésard, S. Hébert, and A. Maignan, Large anisotropic thermal conductivity of the intrinsically two-dimensional metallic oxide PdCoO<sub>2</sub>, *Phys. Rev. B* **91**, 041113 (2015).
- [17] H.-J. Noh, J. Jeong, J. Jeong, E.-J. Cho, S. B. Kim, K. Kim, B. I. Min, and H.-D. Kim, Anisotropic Electric Conductivity of Delafossite PdCoO<sub>2</sub> Studied by Angle-Resolved Photoemission Spectroscopy, *Phys. Rev. Lett.* **102**, 256404 (2009).
- [18] M. Hasegawa, M. Tanaka, T. Yagi, H. Takei, and A. Inoue, Compression behavior of the delafossite-type metallic oxide PdCoO<sub>2</sub> below 10 GPa, *Solid State Commun.* **128**, 303 (2003).
- [19] R. D. Shannon, C. T. Prewitt, and D. B. Rogers, Chemistry of noble metal oxides. II. Crystal structures of platinum cobalt dioxide, palladium cobalt dioxide, copper iron dioxide, and silver iron dioxide, *Inorg. Chem.* **10**, 719 (1971).
- [20] H. Takatsu, S. Yonezawa, S. Mouri, S. Nakatsuji, K. Tanaka, and Y. Maeno, Roles of High-Frequency Optical Phonons in the Physical Properties of the Conductive Delafossite PdCoO<sub>2</sub>, *J. Phys. Soc. Jpn.* **76**, 104701 (2007).
- [21] T. Harada, K. Sugawara, K. Fujiwara, M. Kitamura, S. Ito, T. Nojima, K. Horiba, H. Kumigashira, T. Takahashi, T. Sato, and A. Tsukazaki, Anomalous Hall effect at the spontaneously electron-doped polar surface of PdCoO<sub>2</sub> ultrathin films, *Phys. Rev. Res.* **2**, 013282 (2020).
- [22] T. Harada, K. Fujiwara, and A. Tsukazaki, Highly conductive PdCoO<sub>2</sub> ultrathin films for transparent electrodes, *APL Mater.* **6**, 046107 (2018).
- [23] M. Brahlek, G. Rimal, J. M. Ok, D. Mukherjee, A. R. Mazza, Q. Lu, H. N. Lee, T. Z. Ward, R. R. Unocic, G. Eres, and S. Oh, Growth of metallic delafossite PdCoO<sub>2</sub> by molecular beam epitaxy, *Phys. Rev. Mater.* **3**, 093401 (2019).
- [24] P. Yordanov, W. Sigle, P. Kaya, M. E. Gruner, R. Pentcheva, B. Keimer, and H.-U. Habermeyer, Large thermopower anisotropy in PdCoO<sub>2</sub> thin films, *Phys. Rev. Mater.* **3**, 085403 (2019).
- [25] J. Sun, M. R. Barone, C. S. Chang, M. E. Holtz, H. Paik, J. Schubert, D. A. Muller, and D. G. Schlom, Growth of PdCoO<sub>2</sub> by ozone-assisted molecular-beam epitaxy, *APL Mater.* **7**, 121112 (2019).
- [26] R. Wei, P. Gong, M. Zhao, H. Tong, X. Tang, L. Hu, J. Yang, W. Song, X. Zhu, and Y. Sun, Solution-Processable Epitaxial Metallic Delafossite Oxide Films, *Adv. Funct. Mater.* **30**, 2002375 (2020).
- [27] T. Kawamoto, A. Krishnadas, C.-H. Hsu, M. Pardo-Almanza, Y. Fujisawa, G. Chang, T. Harada, and Y. Okada, Visualization of robust two-dimensional bulk states with suppressed surface state on epitaxial PdCoO<sub>2</sub> thin films with bipolar surfaces, *Phys. Rev. Mater.* **7**, 024001 (2023).
- [28] Q. Song, J. Sun, C. T. Parzyck, L. Miao, Q. Xu, F. V. E. Hensling, M. R. Barone, C. Hu, J. Kim, B. D. Faeth, H. Paik, P. D. C. King, K. M. Shen, and D. G. Schlom, Growth of PdCoO<sub>2</sub> films with controlled termination by molecular-beam epitaxy and determination of their electronic structure by angle-resolved photoemission spectroscopy, *APL Mater.* **10**, 091113 (2022).
- [29] Q. Song, Z. He, B. D. Faeth, C. T. Parzyck, A. Scheidt, C. J. Mowers, Y. Feng, Q. Xu, S. Hasko, J. Park, M. R. Barone, Y. E. Suyolcu, P. A. van Aken, B. Pamuk, C. J. Fennie, P. D. C. King, K. M. Shen, and D. G. Schlom, Surface reconstructions and electronic structure of metallic delafossite thin films, *APL Mater.* **12**, 081117 (2024).
- [30] T. Harada and A. Tsukazaki, Control of Schottky barrier height in metal/ $\beta$ -Ga<sub>2</sub>O<sub>3</sub> junctions by insertion of PdCoO<sub>2</sub> layers, *APL Materials* **8**, 041109 (2020).
- [31] T. Harada and A. Tsukazaki, Dynamic characteristics of PdCoO<sub>2</sub>/ $\beta$ -Ga<sub>2</sub>O<sub>3</sub> Schottky junctions, *Appl. Phys. Lett.* **116**, 232104 (2020).
- [32] T. Harada, Thin-film growth and application prospects of metallic delafossites, *Mater. Today Adv.* **11**, 100146 (2021), and references therein.
- [33] P. F. Carcia, R. D. Shannon, P. E. Bierstedt, and R. B. Flippen, O<sub>2</sub> Electrocatalysis on Thin Film Metallic Oxide Electrodes with the Delafossite Structure, *JES* **127**, 1974 (1980).
- [34] T. Harada, T. Nagai, M. Oishi, and Y. Masahiro, Sputter-grown c-axis-oriented PdCoO<sub>2</sub> thin films, *J. Appl. Phys.* **133**, 085302 (2023).
- [35] T. Harada, P. Bredol, H. Inoue, S. Ito, J. Mannhart, and A. Tsukazaki, Determination of the phase coherence length of PdCoO<sub>2</sub> nanostructures by conductance fluctuation analysis, *Phys. Rev. B* **103**, 045123 (2021).
- [36] N. Nandi, T. Scaffidi, P. Kushwaha, S. Khim, M. E. Barber, V. Sunko, F. Mazzola, P. D. C. King, H. Rosner, P. J. W. Moll, M. König, J. E. Moore, S. Hartnoll, and A. P. Mackenzie, Unconventional magneto-transport in ultrapure PdCoO<sub>2</sub> and PtCoO<sub>2</sub>, *npj Quantum Mater.* **3**,

- 66 (2018).
- [37] J. H. Lee, T. Harada, F. Trier, L. Marcano, F. Godel, S. Valencia, A. Tsukazaki, and M. Bibes, Nonreciprocal transport in a rashba ferromagnet, delafossite  $\text{PdCoO}_2$ , *Nano Lett.* **21**, 8687 (2021).
  - [38] P. Ngabonziza, A. Sharma, A. Scheid, S. Sajeev, P. A. van Aken, and J. Mannhart, Magnetotransport properties of epitaxial films and hall bar devices of the correlated layered ruthenate  $\text{Sr}_3\text{Ru}_2\text{O}_7$ , *Phys. Rev. Mater.* **8**, 044401 (2024).
  - [39] See Supplemental Material at ... for details regarding the design of the Hall bar devices and the acquisition of the STEM data. Atomic force microscopy data as well as complementary XRD rocking curves, magnetotransport and electronic transport data are provided.
  - [40] S. Acharya, A. Chatterjee, V. Bhatia, A. I. K. Pillai, M. Garbrecht, and B. Saha, Twinned growth of ScN thin films on lattice-matched GaN substrates, *Mater. Res. Bull.* **143**, 111443 (2021).
  - [41] S. Dolabella, A. Borzì, A. Dommann, and A. Neels, Lattice strain and defects analysis in nanostructured semiconductor materials and devices by High-Resolution X-ray diffraction: Theoretical and practical aspects, *Small Methods* **6**, 2100932 (2022).
  - [42] A. Scheid, T. Heil, Y. E. Suyolcu, N. Enderlein, A. P. N. Tchiomo, P. Ngabonziza, P. Hansmann, D. G. Schlom, P. A. van Aken, *et al.*, Unveiling the interfacial reconstruction mechanism enabling stable growth of the delafossite  $\text{PdCoO}_2$  on  $\text{Al}_2\text{O}_3$  and  $\text{LaAlO}_3$ , *ACS Appl. Mater. Interfaces* (2025).
  - [43] J. M. Ok, M. Brahlek, W. S. Choi, K. M. Roccapiore, M. F. Chisholm, S. Kim, C. Sohn, E. Skoropata, S. Yoon, J. S. Kim, *et al.*, Pulsed-laser epitaxy of metallic delafossite  $\text{PdCrO}_2$  films, *APL Mater.* **8**, 051104 (2020).
  - [44] J. Roudebush, N. H. Andersen, R. Ramlau, V. O. Garlea, R. Toft-Petersen, P. Norby, R. Schneider, J. Hay, and R. Cava, Structure and magnetic properties of  $\text{Cu}_3\text{Ni}_2\text{SbO}_6$  and  $\text{Cu}_3\text{Co}_2\text{SbO}_6$  delafossites with honeycomb lattices, *Inorg. Chem.* **52**, 6083 (2013).
  - [45] A. P. Nono Tchiomo, E. Carleschi, A. R. Prinsloo, W. Sigle, P. A. Van Aken, J. Mannhart, P. Ngabonziza, and B. P. Doyle, Combined spectroscopy and electrical characterization of  $\text{La:BaSnO}_3$  thin films and heterostructures, *AIP Adv.* **12**, 105019 (2022).
  - [46] A. P. Nono Tchiomo, W. Braun, B. P. Doyle, W. Sigle, P. Van Aken, J. Mannhart, and P. Ngabonziza, High-temperature-grown buffer layer boosts electron mobility in epitaxial La-doped  $\text{BaSnO}_3/\text{SrZrO}_3$  heterostructures, *APL Mater.* **7**, 041119 (2019).
  - [47] A. P. Nono Tchiomo, *Electronic Band Structure and Transport Studies of Oxide Materials* (University of Johannesburg (South Africa), 2020).
  - [48] R. A. Matula, Electrical resistivity of copper, gold, palladium, and silver, *J. Phys. Chem. Ref. Data* **8**, 1147 (1979).
  - [49] M. Cimberle, G. Bobel, and C. Rizzuto, Deviations from Matthiessen's rule at low temperatures: an experimental comparison between various metallic alloy systems, *Adv. Phys.* **23**, 639 (1974).
  - [50] J. Bass, Deviations from Matthiessen's rule, *Adv. Phys.* **21**, 431 (1972).
  - [51] D. Barbalas, A. Legros, G. Rimal, S. Oh, and N. Armitage, Disorder-enhanced effective masses and deviations from Matthiessen's rule in  $\text{PdCoO}_2$  thin films, *Phys. Rev. B* **106**, 115113 (2022).
  - [52] G. Bergmann, Weak localization in thin films: a time-of-flight experiment with conduction electrons, *Phys. Rep.* **107**, 1 (1984).
  - [53] N. Kikugawa, P. Goswami, A. Kiswandhi, E. Choi, D. Graf, R. Baumbach, J. Brooks, K. Sugii, Y. Iida, M. Nishio, *et al.*, Interplanar coupling-dependent magnetoresistivity in high-purity layered metals, *Nature Commun.* **7**, 10903 (2016).
  - [54] T. Harada, P. Bredol, H. Inoue, S. Ito, J. Mannhart, and A. Tsukazaki, Determination of the phase coherence length of  $\text{PdCoO}_2$  nanostructures by conductance fluctuation analysis, *Phys. Rev. B* **103**, 045123 (2021).
  - [55] C. Shekhar, A. K. Nayak, Y. Sun, M. Schmidt, M. Nicklas, I. Leermakers, U. Zeitler, Y. Skourski, J. Wosnitza, Z. Liu, *et al.*, Extremely large magnetoresistance and ultrahigh mobility in the topological weyl semimetal candidate NbP, *Nature Phys.* **11**, 645 (2015).